CONF-9[illegible] DOE/ET/10815--149

DE90 012632

CHARACTERIZATION OF FLOW DISTURBANCES IN A COAL FIRED COMBUSTION FLOW TRAIN

B. C. Winkleman, T. V. Giel, J. T. Lineberry, and D. J. Yang
The University of Tennessee Space Institute
Tullahoma, TN

ABSTRACT

Audible rumbles are known to accompany operation of the CFFF low mass flow train and visual/aural observations indicate simultaneous dropouts in the diffuser light emission. Three hypotheses, coal flow disturbances, combustion instabilities, and slag entrainment into the flow, are presented as possible causes of the rumbles. Wideband instrumentation including line reversals, luminosities, and dynamic pressures were used to investigate the rumble phenomena. The observational evidence implies that briefly before the rumble sound, the vitiation heater pressure rises and a cold opaque structure moves from upstream to downstream through the aerodynamic duct, diffuser, and radiant furnace. Steady state thermodynamic analysis of the flow train at conditions corresponding to measured rumble phenomena are presented. It is concluded that a dispersed structure of slag particles entrained from the combustor is the most viable hypothesis.

INTRODUCTION

The Coal Fired Flow Facility (CFFF) has exhibited flow disturbances that are characterized by easily audible acoustic rumbles during coal operation of the LMF flow train. The loudness and frequency of occurrence of the rumbles varies and has reached sufficient intensity and repetition that CFFF operators have temporarily shut down the flow train during long duration testing. Although the rumbles have been noted over a period of several years, no extensive study of the phenomena has previously been carried out, although the disturbances were discussed with regard to the uncertainty of the modified line reversal temperature measurements made by the University of Tennessee Space Institute (UTSI).[1] The purpose of the this study was the analysis of quantitative measurements that could identify the underlying cause of the flow disturbances with the goal of ultimately eliminating the phenomena.

The rumbles were first quantitatively measured with the UTSI spectrometer line reversal system which has a time resolution on the order of 1 ms for temperature readings and on the order of 10 μs for optical emission measurements. Figure 1 gives time traces of the spectrometer line reversal signals during a typical event. The rumble event is characterized in the line reversal signals as a significant drop in the intensity of radiation from both the gas, I_{pl}, and the lamp plus gas, I_{pl+l}, indicating a simultaneous loss in both gas emissivity and transmissivity. Most of the drop seen in Figure 1 occurs over

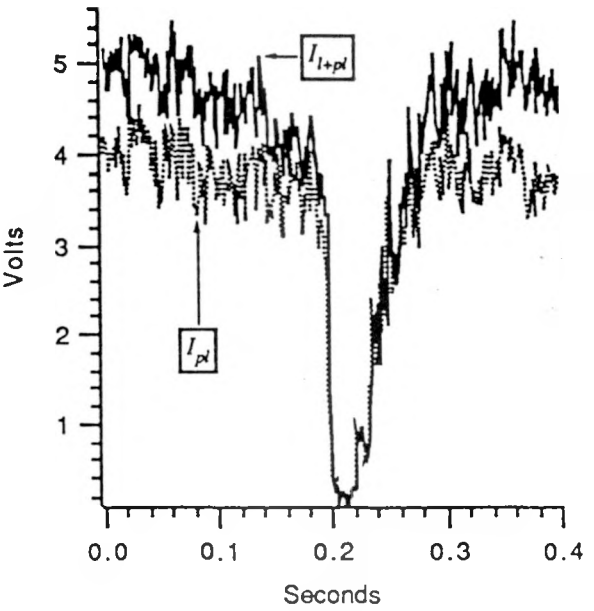

Figure 1. Typical Dropouts Seen in the Line Reversal Signals During a Rumble Event.

a period of less than 100 ms, which clearly demonstrates the need for wide band diagnostics to adequately resolve the event and characterize the phenomena.

The rumble phenomenon could produce fatigue stresses in the LMF flow train, possibly leading to hardware failures. However, examination of the downstream CFFF hardware does not indicate that any damage has been done by the rumble thus far. Of course the rumble could also change the electrical output of an MHD generator, if the rumble propagates through the MHD generator.

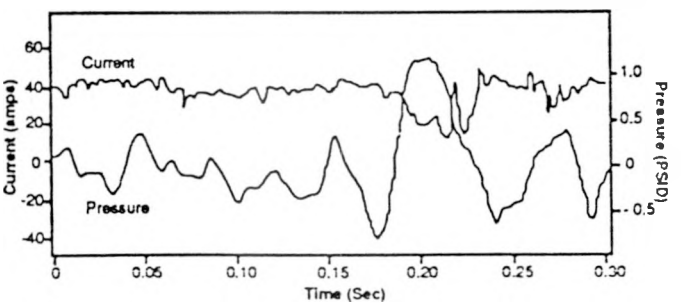

Figure 2. Comparison of Combustor Pressure Rise and Generator Current Drop from a TP40 Test.

*This work was supported by the Department of Energy under contract DE-AC02-79ET-10815. Paper DOE/ET/10815-149.

No generator is in operation at the CFFF, but earlier UTSI generator tests did show random current "dropouts" as illustrated in Figure 2.[2] Because only very limited wide band data acquisition, processing, and analysis capabilities existed at UTSI during these pre-CFFF tests, resolution of the causes of these dropouts was not possible during these generator tests, and it is not known if any relationship exists between these earlier observations and the current rumble. Nevertheless, the similarity of the dynamic pressure increase seen with the rumble event and that seen in Figure 2 suggest the same phenomena.

Several causes for the rumble have been hypothesized. The first suggested cause is coal flow disturbances. Dense phase solids flow is not as are easily controlled as gas or liquid flows, but improvements in the CFFF coal transport stability have not appeared to decrease the rumble intensity or frequency. However stable coal-seed flow may not mean stable coal flow if the coal and seed segregate. Another possible cause for the rumble is combustion instability,[3,4] including severe instabilities such as periodic flame out. The final hypothesis is periodic slag entrainment into the flow field with subsequent partial flow blockage from the 100% slag carry over combustor used at the CFFF. Wideband instrumentation was employed to assist in delineating between these possibilities and to help identify additional possible causes.

Because of the acoustic nature of the rumble, the flow train was instrumented with a microphone and four helium bleed dynamic pressure transducers to quantify the fluctuation pressures associated with the rumble. In addition, recent visual/aural observations indicated a correlation existed between the rumbles and large drops in the intensity of visible light emanating from the diffuser optical diagnostic ports. Thus, two luminosity sensors were installed to help measure the rumble along with the three CFFF high frequency line reversal sensors.

Table 1 describes the diagnostic devices used in the study. A schematic of the CFFF flow train showing the locations of these diagnostics is given in Figure 3. Data was acquired and processed using the CFFF Masscomp/Concurrent MC5400 computer system. The system allows up to 64 data channels to be digitized at 12 bit resolution, with up to 32 of those channels simultaneously sampled. The aggregate data rate is 1.0 megasamples per second to memory, and 0.75 megasample per second directly to a high speed mass storage disk drive. Data acquisition hardware is controlled using custom software and Laboratory Workbench (LWB) which is a commercial product of Masscomp/Concurrent. Data analysis was performed using custom software, LWB, the IEEE library of digital signal analysis algorithms and National Instruments™ LabVIEW Software, the control and analysis software package for the UTSI high frequency line reversal system.

A major portion of the transient data being addressed herein was taken from measurements made during a short period in the LMF4-S test. This period was between 23:30 and 24:00 on Dec 5, 1989. During this time period quality rumble data were recorded and operation of the LMF test train as a whole was held very stable. A summary of the combustor operating

Table 1
Diagnostics used to Characterize Disturbance Phenomena

Device	N	Freq	Location	Comments
Line Reversal	3	1 kHz (Temp) 100 kHz (Emiss)	Diffuser (2) Radiant Furnace	The two diffuser systems measure the same spatial location but can be used at different wavelengths.
Helium Bleed Pressure Transducers	4	25 kHz Resonant Frequency	Vitiation Heater Duct (2) Diffuser	These are dynamic transducers and communicate directly with the combustion gas.
Microphone	1	20 kHz	Radiant Furnace	This device measured the audible boom.
Luminosity Probes	2	5 kHz	Duct (2)	Cross correlation between probes allows measurement of disturbance velocity.

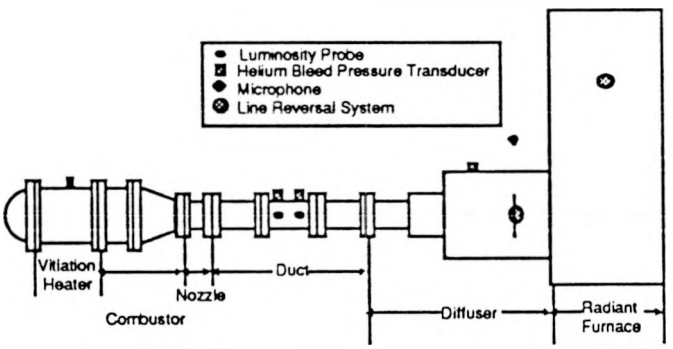

Figure 3. Flow Train Schematic Showing Locations of Diagnostics

parameters that were measured during this period of LMF4-S is presented in Table 2. As can be seen in this table, during this test period the LMF test train was sustained at a condition which is representative of its nominal 19 MW_t base operating condition but slightly lower in terms of reactant flow rates. The base operating point that is tabulated represents that nominal objective point as set in the pretest run schedule; whereas the reactant flow data represent the recorded measured flows during the subject time period .

OBSERVATIONS

The diagnostics described in Table 1 were used during test LMF4-S at the CFFF. All instrumentation worked well with the exception of the two helium bleed pressure transducers located in the duct. These two transducers appeared to be plugged with slag during the data collection periods; however, they were not installed to allow direct communication with the gas which may have reduced their

TABLE 2
CFFF LMF COMBUSTOR OPERATING POINT
(Experimental Data of LMF4-S, Time Period: 155.5 to 155.75 Hours)

	Reactants Flows (kg/s)	Base
Coal - Illinois #6	0.357	0.381
Seed - K2CO3	0.044	0.047
Oil - (#2 Fuel Oil)	0.180	0.193
Air	1.480	1.539
Oxygen	0.820	0.824
Nitrogen (Carrier)	0.020	0.021
Total Flow	2.901	3.005
Set Point		
Stoichiometry	0.84	0.85
N/O (mass)	1.00	1.00
Thermal Input	18.2 MWt	19 MWt
Combustion Pressure	4.25 Atm	4.5 Atm
Heat Loss (Combustor-Nozzle)	1.41 MW_t	1.42 MW_t

response to below the measurement threshold. Data was collected during six periods near the end of LMF4-S. Individual disturbance events were recorded by triggering the data acquisition system on drops in the diffuser line reversal signals. Approximately 300 events were accumulated during the six periods which covered a total time of 42 minutes. Data from typical events that elucidate the general character of the disturbances are presented in this paper. Some statistical analysis of the events are also presented but complete stochastic analyses of all the events have not been completed.

Since data from typical events are presented in this paper, clarification of the definition of a typical event is required. Examination of time traces of the signals allowed the events to be classified according to their general shape. While there was great variety in the recorded waveforms of the various parameters, most events displayed similar temporal structure. The pertinent features of a luminosity signal during a typical event are shown schematically in Figure 4. Luminosity signals were used as the basis for classification of the events because they showed the most definitive and varied structure. Two other classifications, denoted as "multiple" and "erratic", are also shown in this figure. In all cases the primary indication of an event was a drop in the mean levels of the luminosity signals.

The time period shown in Figure 4 has been divided into three intervals covering the periods before, during, and after the event. The trace of the luminosity signal during the pre and post event periods shows the normal behavior of random fluctuations around a fairly constant mean (a stationary stochastic process). During the event period of a typical dropout, the luminosity signal would quickly drop to zero and would remain at the zero level minimum for a period normally between 5 and 20 ms. The signal would then recover

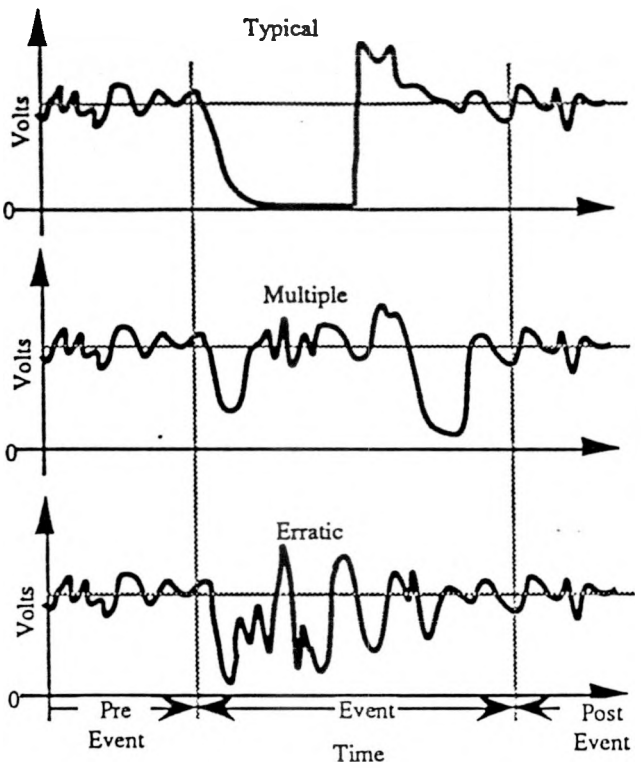

Figure 4. Classification of Rumble Events

abruptly, reaching a level significantly greater then the average level of the signal in the pre and post event periods. As shown in Figure 4, the recovery of the luminosity signal was faster then its drop.

The events classified as "multiple" consisted of two or more individual events close together in time (< .5 sec). Normally each event would be distinct (non-overlapping) and not as severe as a typical event as characterized by dropout depth and width. The final classification of "erratic" included events which were clearly not single or distinct dropouts. In these events, signal levels fluctuated randomly such as during the pre and post event periods; however, the fluctuation levels had significantly greater amplitudes during the event period. It is possible that erratic events consisted simply of brief, multiple, and partially overlapped events.

Of 140 events classified in this manner 61% were typical, 16% were multiple, and the remaining 23% were erratic. It should be noted that the events examined were preselected from all possible events by the data acquisition process which only recorded events of a specified and arbitrary severity. The severity measure for data acquisition was based on the diffuser line reversal signal, I_{pl+l}, and was chosen such that events that caused a drop in I_{pl+l} to levels less then 1/4 of its nominal value were recorded. This level minimized the number of false triggerings caused by the normal stochastic fluctuations of I_{pl+l} while maximizing the number of rumble events recorded.

Throughout the remainder of this paper, event and typical event can be considered synonymous since all presented data will be drawn from events classifiable as typical.

General.

The acoustic noise which is the signature characteristic of the rumble events is easily audible throughout the downstream area of the CFFF flow train even though ambient noise conditions are quite high. Aural observations have proven insufficient to locate the point of origin of the sound. Close visual scrutiny of the visible light emanating from diffuser optical ports shows a definite correlation between the audible rumble and severe drops in the light intensity.

The rumbles appear to be periodic when observable. Examination of the times of the recorded events of this study show a mean period between events of 7.5 seconds with a standard deviation of 1.2 seconds. The maximum time period was 10 seconds and the minimum was 5. The narrow range of observed event separations suggest a deterministic as opposed to random phenomena. There is evidence that the mean period between events is not constant.

Line Reversal.

Gas temperature measurements were made in the diffuser using spectrometer and photodiode based temporal separation modified line reversal systems. The optical configuration of the system, shown in Figure 5, allowed simultaneous measurements of temperature and transmission at two wavelengths. A beamsplitter placed just before the photodiode detector head diverted half of the radiation from the gas/reference source to the entrance slit of the spectrometer. Thus the photodiode detector and the spectrometer made measurements on the same light path. The photodiode based system used an interference filter with a 1 nm bandpass centered at 750 nm. Since the wavelength of the photodiode line reversal was fixed, it was always used to monitor the potassium emission due to the 767/ 770 nm doublet. Under normal operating conditions, the radiation from this doublet is sufficiently broadened to emit strongly at 750 nm. The spectrometer wavelength setting was remotely controllable and thus could be set to other wavelengths than 750 nm for simultaneous measurements at different wavelengths. The spectrometer could also be scanned to obtain the emission/transmission spectrum of the gas. The chopper on the source side allowed separation of I_{pl} and I_{pl+l}.

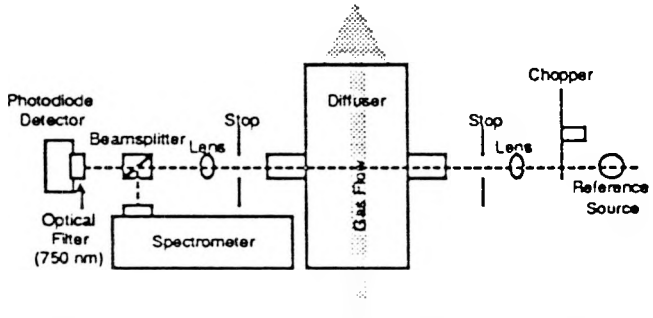

Figure 5. Overhead View of Diffuser Line Reversal Optical System.

A third line reversal system was used on the radiant furnace. This was a photodiode system using 750 nm interference filters but configured to spatially separate I_{pl} and I_{pl+l}.

The frequency response of the diffuser line reversal systems was primarily limited by the chopping rate which was 1 kHz. Temperature and transmission determinations are limited to this rate. However, information about emission fluctuations is available up to approximately 100 kHz which is the limit of the photomultiplier tube and amplifier of the spectrometer. The line reversal system used on the radiant furnace was frequency limited only by the bandpass of the photodiode detector and associated electronics which was about 5 kHz.

The diffuser spectrometer line reversal system was used to trigger the acquisition of individual events. Drops in the intensity of I_{pl+l} initiated a data acquisition covering a period of one second. The pretigger interval of recorded data was .2 seconds. In general, all data is presented such that the trigger point occurs at zero.

Traces of the diffuser spectrometer line reversal signals during a typical event is shown in Figure 6. For this event the spectrometer wavelength setting was 750 nm. The transmission, τ, of the gas is given by

$$\tau = \frac{I_{pl+l} - I_{pl}}{I_l}$$

where I_l is a constant calibration quantity. Clearly the traces of Figure 6 show the transmission decreasing substantially during the event. In this figure the signals fall more rapidly than they recover which is normal behavior of the line reversal signals during an event.

Figure 7 gives the calculated transmission through the event of Figure 6. The transmission drops more rapidly than the traces of Figure 6 since I_{pl+l} approaches I_{pl} as the magnitude of both fall. At minimum, the transmission reaches zero implying the gas has become opaque at 750 nm.

The average transmission value during the post event period of Figure 7 is .30 with a standard deviation of .09 which is representative of the gas transmission at 750 nm during normal CFFF operating conditions.

The temperature of the gas, T, through the event can be obtained from the standard line reversal equation

$$T = \frac{T_s}{1 - \frac{\lambda T_s}{C_2} ln\left(\frac{k I_{pl}}{I_{pl} + I_l - I_{l+pl}}\right)}$$

where T_s is the brightness temperature of the reference source at the measurement wavelength of λ, C_2 is the second radiation constant, and k is optical system calibration factor.

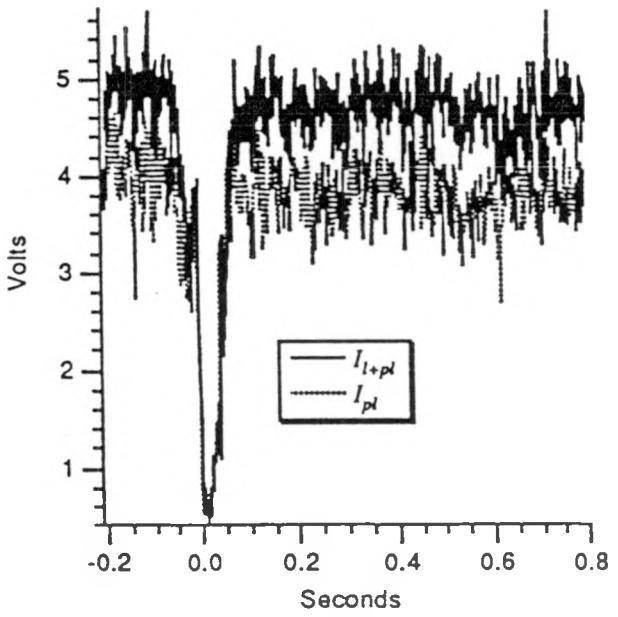

Figure 6. Spectrometer Diffuser Line Reversal Signals at 750 nm During Typical Event

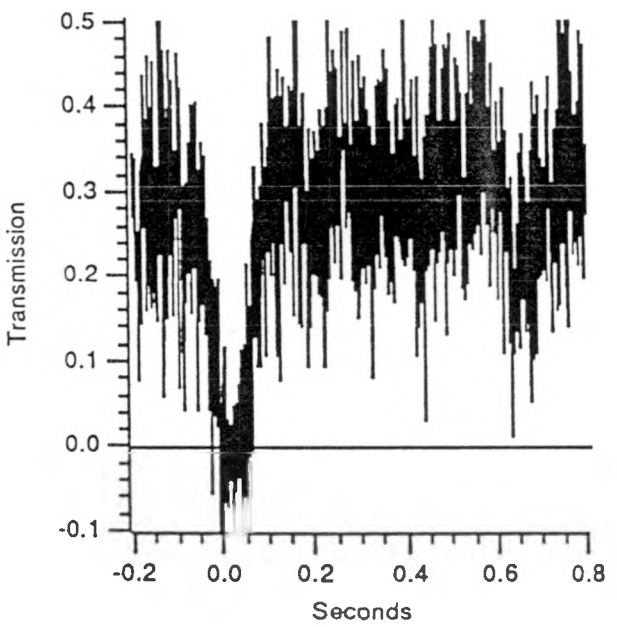

Figure 7. Gas Transmission at 750 nm During Typical Event

Using the data of Figure 6 the temperature change of the gas through a typical event can be calculated. The result is presented in Figure 8. The temperature drops severely reaching a minimum of about 1900 K. For comparison the temperature in the post event interval was 2520 K with a standard deviation of 38 K indicating a 600 K drop in the gas temperature through the event. The full width at half maximum of this event was about 40 ms. The total time period of the event is less well defined but was approximately 130 ms.

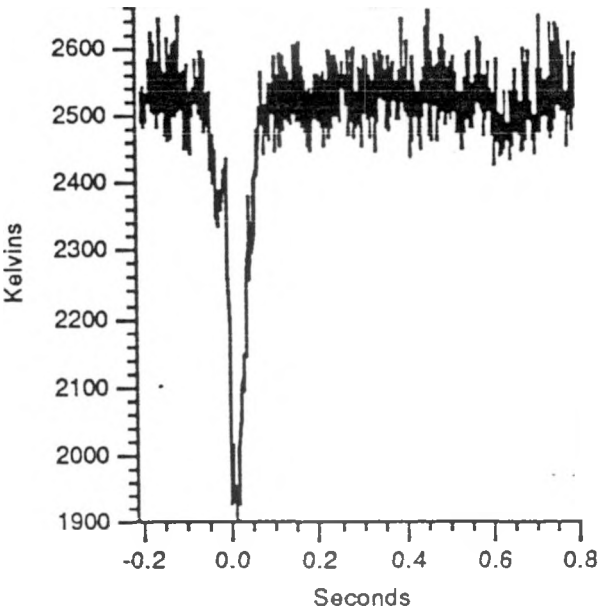

Figure 8. Diffuser Temperature Variation Through an Event.

The actual minimum temperature reached during the event may be significantly lower than 1900 K due to increased measurement error at low temperatures. This increased error is caused by the exponential variation of emitted light intensity versus temperature giving line reversal systems a relatively narrow temperature measurement range. The variation in intensity is particularly bothersome as the temperature falls since the signal to noise ratio quickly becomes too poor for accurate temperature determinations. This problem is evident in the Figure 7 where the gas transmission at the minimum is frequently less than zero which is not possible. Sources of noise of fixed magnitude (not proportional to signal levels) caused by detector dark current, amplifier noise, etc. produce an operational lower temperature limit below which a line reversal system cannot measure. For the diffuser line reversal systems optimized for the expected diffuser temperature, this lower limit is near 1900 K. The nominal temperature accuracy of the diffuser line reversal systems is ± 50 K for temperatures greater than 2100 K.

In Figure 9 two typical events are shown that allow comparison of I_{pl+l} and I_{pl} at different wavelengths. The signals from the diffuser photodiode line reversal (fixed at 750 nm) are shown with the simultaneously measured spectrometer signals for wavelengths of 589 nm (near the Na emission doublet) and 650 nm (which is not near any strong resonant emission line). For the photodiode traces in Figure 9, zero light intensity occurs at -7 volts.

Comparison of the traces in Figure 9 shows similar behavior during each event at the different photodiode and spectrometer wavelengths. A high degree of correlation is seen between the 750 nm and 589 nm signals which are both due to resonant absorption. Comparison of the 650 and 750 nm signals show that they are different in the pre and post event periods. During these periods reduced emission and increased

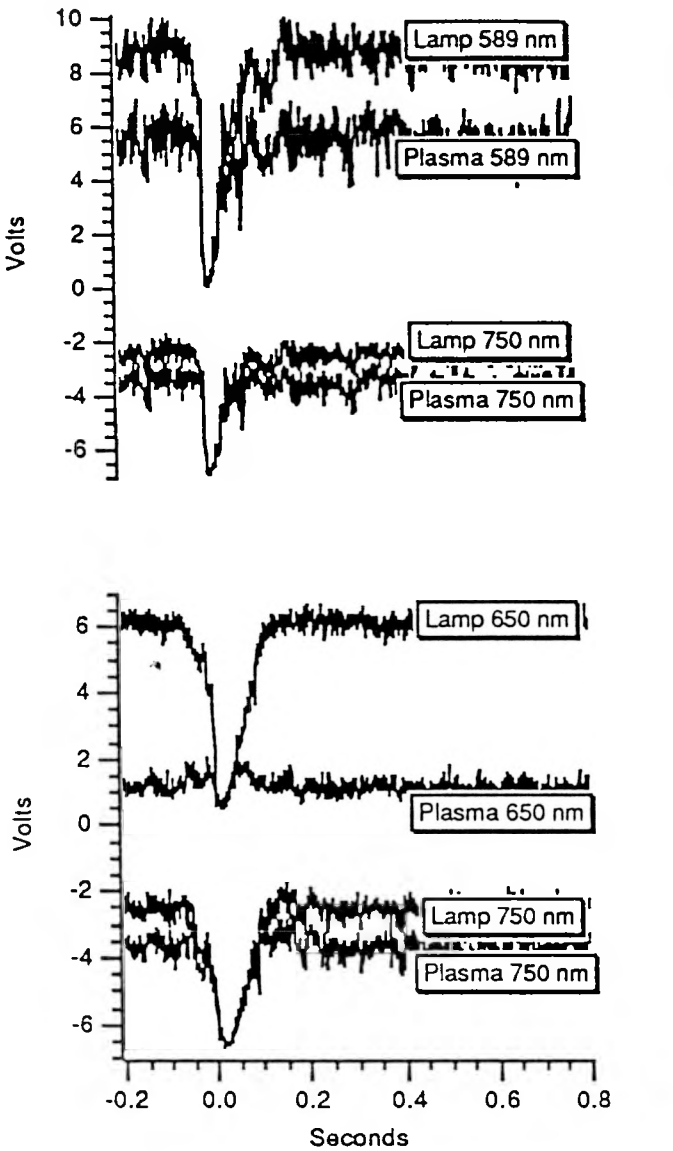

Figure 9. Comparison of Line Reversal Signals at Different Wavelengths.

transmission at 650 nm is indicated. However the event is still clearly evident at 650 nm as indicated by drops in the signal levels

Importantly, the line reversal traces indicate a drop in temperature and near zero transmission at all three wavelengths. Thus the phenomena causing the transmission decrease is broad band indicating particulate absorption/scattering as opposed to resonant line absorption which would have much narrower spectra.

The conclusion from the diffuser line reversal measurements is that during an event the line reversal systems see a cold, opaque, and probably particulate laden gas. A coal flow disturbance, such as a brief interruption by blockage at the injector or an increase in the seed/coal ratio, would not generate the measured line reversal signals at all wavelengths. However, a large rapid increase in the coal/seed flow rate could account for the broad band absorption by introduction of a large number of particles. Such an increase is considered to be unlikely since mechanisms for driving the increase would be detected by coal transient pressure and flow monitoring devices. (Brief blockage at the injector is not detectable with current instrumentation due to a choking restriction in the feed line.) A loss of combustion of the coal or slag entrainment into the flow from the combustor could account for the observed diffuser waveforms in a similar manner by the introduction of a cloud of particles into the flow train.

Examples of the radiant furnace line reversal signals (I_{pl+l} and I_{pl}) are given in Figure 10. The greatest effect of the event on these signals shows up primarily as a depressed I_{pl+l} signal though I_{pl} is also affected. In comparison to the diffuser signals, the furnace effect begins later (at about .17 seconds) and lasts longer (neither signal has recovered by the end of the plot at .8 seconds). Also the magnitude of the drop is not as great being only about 40 % for I_{pl+l} and about 25% for I_{pl} . In comparison the drops in both I_{pl+l} and I_{pl} at the diffuser for all wavelengths was nearly 100%. The calculated transmission and temperature functions are given in Figure 11. The temperature falls 75 K from the pre event average of 1875 K to the minimum recorded temperature of 1800 K occurring at .4 sec after detection of an event in the diffuser. The transmission drops from .14 to about .04 during the same interval.

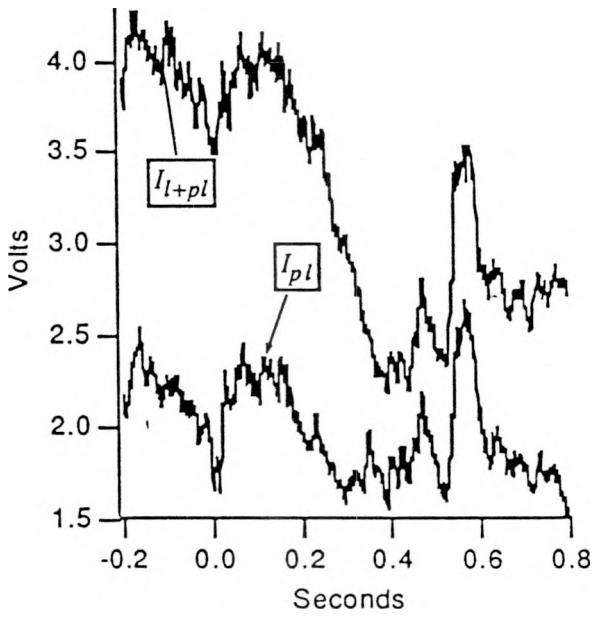

Figure 10. Radiant Furnace Line Reversal Signals During Event.

The temporal ordering between the effects of the event seen in the diffuser and radiant furnace is consistent with a phenomena being convected with the gas and moving from the diffuser into the furnace. Similarly the spreading and dilution of the

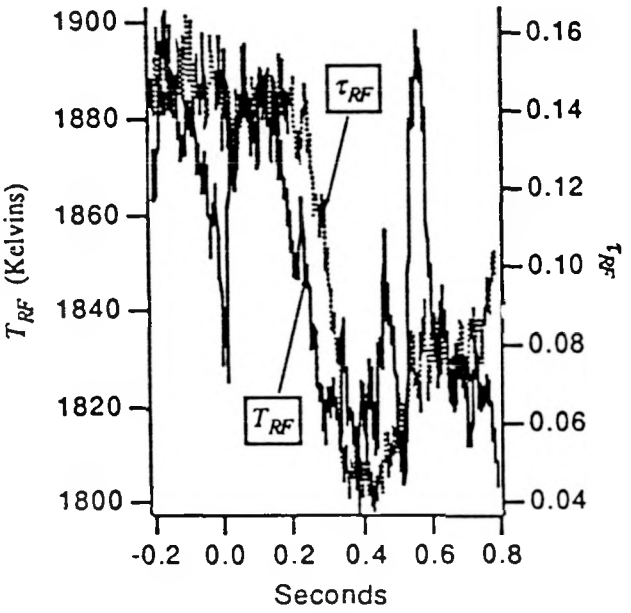

Figure 11. Radiant Furnace Temperature and Transmission Through Event.

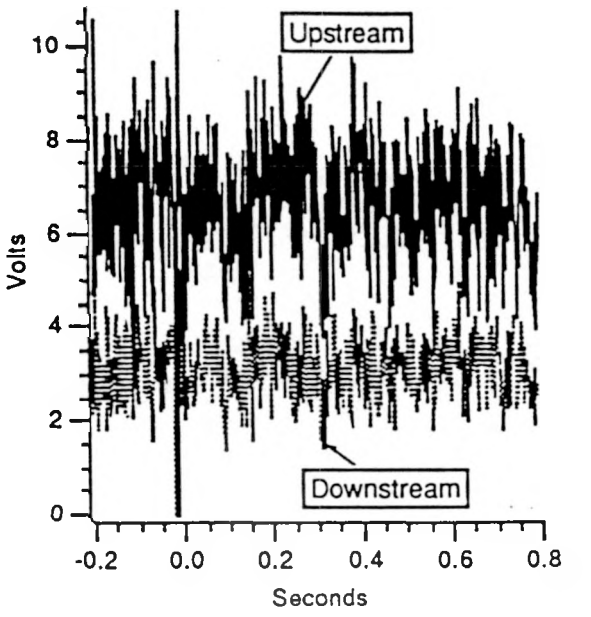

Figure 12. Raw Luminosity Signals During Typical Event.

event in the radiant furnace would be expected from the known flow field recirculation pattern of the radiant furnace[5,6] coupled with the larger volume and thus lower speed of the gas in the furnace. Thus, further support is given to the hypotheses of momentary loss of combustion or slag ejection.

Luminosity

An example of the luminosity signals during an event is given in Figure 12 for the entire one second acquisition period. The raw signal from each of the probes before being corrected for DC offsets and differing sensitivities are plotted in this figure. The effect of the rumble event is evident for only a very brief period just before time zero of the plot. Because the event occurred before time zero (when the event begins in the diffuser) the phenomena must originate upstream of the luminosity probes and move downstream.

There is a high degree of correlation evident between the two signals that suggests the use of cross correlation techniques to evaluate the velocity of the gas. The normalized cross correlation function, $R_{upstream,downstream}$, of the luminosity signals of Figure 12 during the post event period is given in Figure 13. The cross correlation function is of classic shape and clearly indicates a maximum correlation at a time delay, δt, from the upstream to the downstream probe of .3 ms (lag value of 3). The standard technique for obtaining the gas velocity, v, directly from this value and the separation of the probes, L =.4064 m, gives 1354 m/s. However, since the time delay must be an integer multiple of the 0.1 ms sampling time, the precision of this method is poor (± 33%). Fortunately, the time delay between two signals also presents itself as a phase shift that is linear with respect to frequency.[7] A graph of the phase shift, φ, between

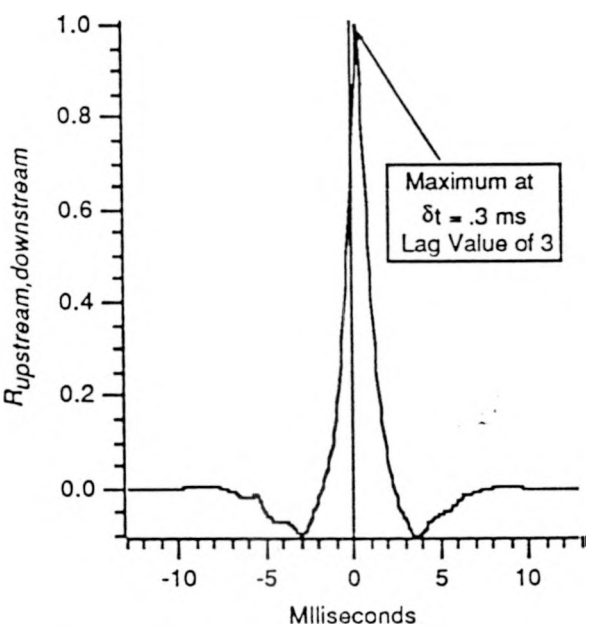

Figure 13. Cross Correlation of Luminosity Signals During Post Event Period.

the two luminosity signals is given in Figure 14. The measured phase shift compares excellently with a linear least square fit also shown on this figure. The time delay is slope/360 when the slope is given in degrees/Hz. This gives a value for δt of .3198 ms implying a gas velocity of 1271 m/s. The average of ten velocity determinations made using the phase shift derived from post event rumble data was 1300 ± 20 m/s.

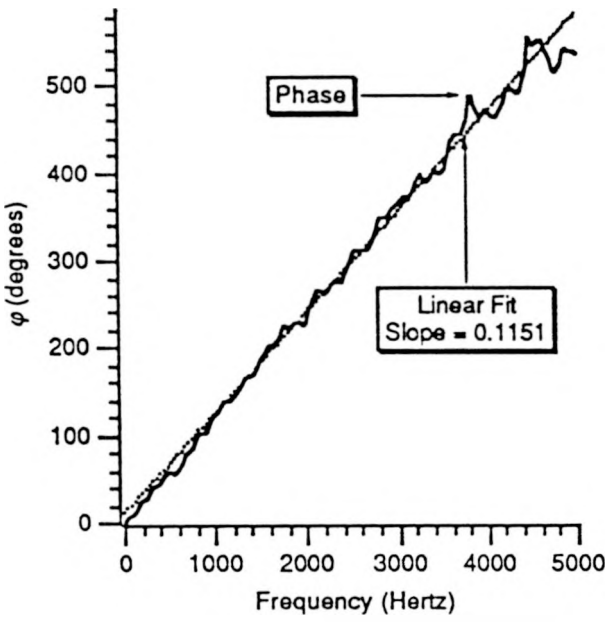

Figure 14. Phase Shift of Luminosity Signals During Post Event Period.

A detail of the luminosity signals during the event is presented in Figure 15. The signals have had their DC offsets removed and have been normalized to the average of the signal during the entire one second data set. Several important characteristics of the changes occurring in the gas due to the rumble event are deducible from this figure. (These characteristics are pertinent only with respect to the gas in the duct region between the nozzle and the shock where aerodynamic conditions remain similar.)

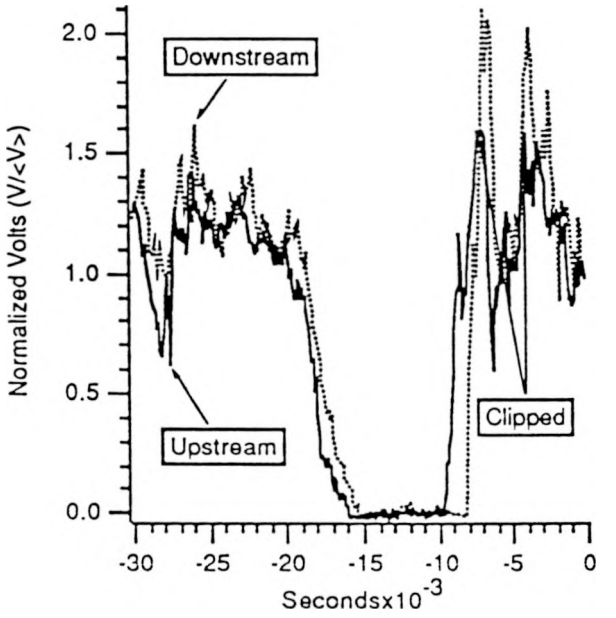

Figure 15. Detail of Luminosity Signals During Event.

Firstly, the temporal ordering of the changes with the downstream probe signal following the upstream probe indicates a structure that moves downstream with the gas. The size of this structure can be estimated from the time period of the dropout and the speed of the gas. For the upstream probe this period is about 11 ms implying a structure length of 14 m using the measured gas velocity of 1300 m/s. It is also possible to estimate the length by comparing the amount of overlap of the two dropout events. Structure lengths of less than (greater than) the probe separation would be expected to produce non-overlapping (overlapping) dropouts. The traces shown in Figure 15 have extensive overlap indicating a structure much larger than the probe separation. The equation for relating the length to the degree of overlap is

$$L = \frac{s}{1 - \frac{\tau}{\tau_0}}$$

where L is the structure length, s is the probe separation, τ is the overlap period, and τ_0 is the width of the dropout at either probe location. This equation produces a value for L of about 8 meters. However, the overlap is difficult to accurately assess due to fluctuations in the falling and rising edges of the signals and the high degree of overlap. Both techniques indicate a length greater than the duct length of 3.0 m.

The above determinations of structure length depended on the structure moving at the gas velocity or at least at constant velocity for the degree of overlap technique. Close examination of Figure 15 reveals that neither situation can be correct since a constant velocity would produce upstream and downstream dropouts of equal length and the downstream dropout is seen to be significantly greater than that of the upstream. The suggestion is that the front edge of the structure is traveling faster than the back edge. If the time delay between the falling edges of the traces are used to obtain the front edge velocity, v_f, a value of about the gas velocity (1300 m/s) is obtained. However, if the same technique is applied to the back edge a velocity, v_b), of 300 m/s is obtained. These values have considerable error on the order of ± 33% for v_f and ± 25% for v_b due to the small lag values involved and the difficulty of determining the correct lag time delay due to the shape of the edges. These problems are most acute for the front edge giving it the greater error. Thus, the structure length is somewhat indefinite lying between a maximum of 14 m and a minimum of 3.3 meters.

The traces in Figure 15 also reveal that the signals rebound after passage of the structure to a level about twice the average value of the signals during the pre and post event periods which is 1.0 on this normalized graph. (Note that some regions of the upstream probe signal were limited during the acquisition process. These regions are marked clipped.) This common feature of the luminosity signals after the event suggests either a higher gas emissivity or higher temperature (or a combination of both). If the increase is considered to be due only to temperature, then the increase in temperature can be computed from Planck's blackbody radiation formula if the temperature corresponding to the average signal level is known. The temperature during the high intensity period after the event, T_1, is given by

$$T_1 = \frac{1}{\frac{1}{T_0} + \frac{\lambda k}{h c} \ln\left[\frac{I_0}{I_1}\right]}$$

where T_0 is the average temperature, λ is the wavelength, k is Boltzmann's constant, c is the speed of light, h is Planck's constant, and I_1 and I_0 are the intensities emitted by the gas. Since only the ratio of the intensities appears in the equation, only a relative measure of the intensities is necessary. A plot of Δt (T_1 -T_0) for three values of T_0 is given in Figure 16. From Figure 12 the peak intensity ratio after the event is two which corresponds to a temperature increase of 215 K for T_0 = 2400 K. The low levels of the signals during the minimum of the dropouts preclude using this technique to predict the temperature drop. However, a significantly reduced temperature is indicated.

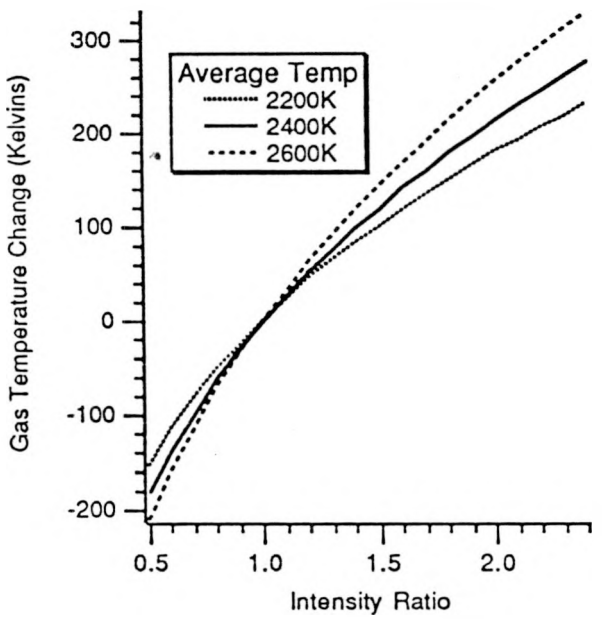

Figure 16. Predicted Temperature Difference.

In summary, the luminosity signals are consistent with the results of the line reversal measurements suggesting a cold structure that moves in the normal gas flow direction. The velocity of the leading and trailing edges appear to be different and the edges are separated by a distance at least as long as the duct. While the slag entrainment hypothesis can adequately explain the emission dropouts, it is impossible that a simple contiguous mass of slag is responsible due to the length of the disturbance. However, a *cloud* of slag particles generated by dispersion due to shear forces as the slag travels through the nozzle could produce such structure lengths. Also, combustion instability or coal flow disturbances could easily account for structures of this length.

One caveat must be given with respect to the above analysis of the luminosity signals. A typical event, as previously defined, was used for this analysis. The main features of the event discussed, such as, leading and trailing edge velocity differences, increased post event luminosity, etc., are general characteristics of typical events. But the range of values exhibited by parameters such as I_1/I_0 have not yet been quantified. More sophisticated techniques, currently under development, are needed to allow thorough examination of a large number of events to statisitically ascertain the average properties.

Pressures

A trace of the vitiation heater dynamic pressure is shown in Figure 16 along with a luminosity signal for temporal reference. There is a rapid and distinct rise in the pressure at the time corresponding to the luminosity dropout. The pressure rise is slightly greater than 1 psi. Vitiation heater pressure increases as great as 5 psi have been observed coincident with rumble events. In general the fluctuations due to rumble events are about twice that of the normal stochastic fluctuations observed in the vitiation heater. Clearly the pressure increase is related in time with the luminosity dropout but the temporal ordering is not definite because of the normal background pressure fluctuations upon which it is superimposed.

Of the suggested hypotheses for the rumble events, only slag entrainment into the flow with subsequent blockage of the flow train can easily explain the consistent vitiation heater pressure *rise* that was observed. A simple model was developed to predict the transient pressure rise. This model assumed a sudden blockage at the nozzle throat and constant mass flow into the vitiation heater/combustor. A predicted rise curve is plotted on Figure 16. The measured and predicted pressure curves match best when a value of .22 is used as the fractional area blockage of the throat. This value is reasonably large enough that audible effects could occur.

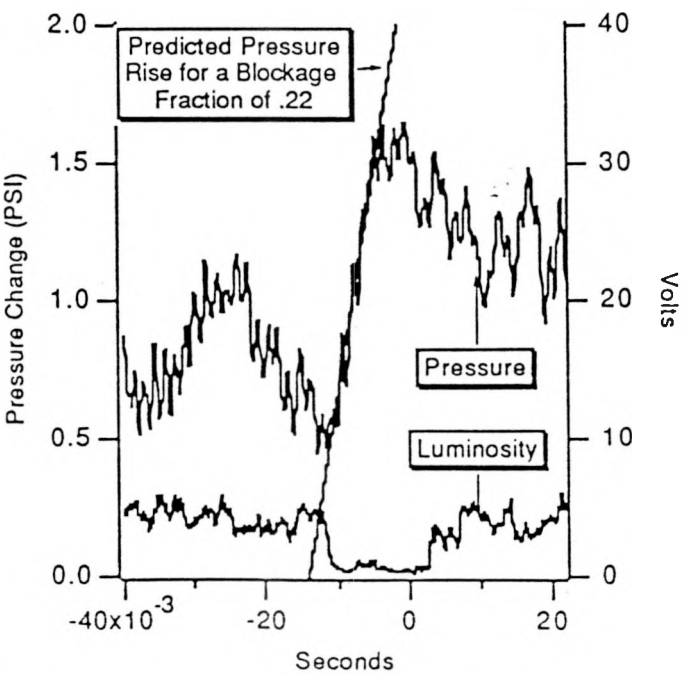

Figure 16. Vitiation Heater Pressure Rise During Event.

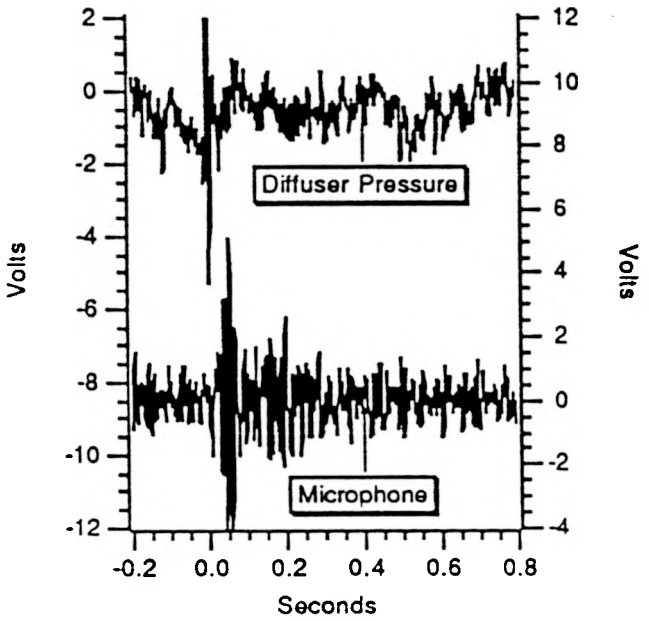

Figure 17. Diffuser Pressure and Microphone Signal During an Event.

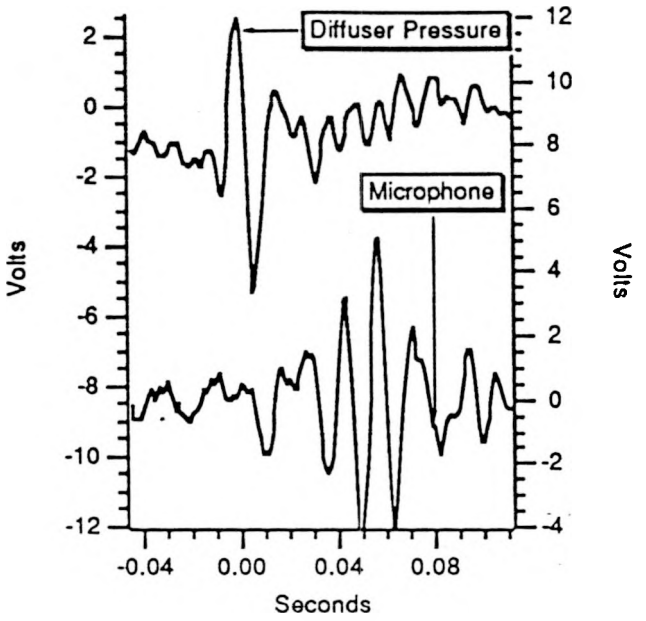

Figure 18. Detail of Diffuser Pressure and Microphone Signal During an Event.

The final rumble observation is presented in Figure 17. This figure which shows traces of the diffuser pressure transient and the microphone signal which shows the pressure wave associated with audible rumble. Details of these pressures are shown in Figure 18. As seen from the figures the sound begins shortly after time zero and is still evident after .3 seconds. The detailed figure reveals the pressure pulse in the diffuser has a simple structure consisting primarily of one cycle of a sinsusoidal signal that begins with a pressure increase. Also, the periods of the diffuser pressure wave and the initial cycles of the audible pressure wave are seen to be approximately equal. The period corresponds to a frequency of 50 Hz.

It is not clear what behavior to expect in the diffuser pressure from the proposed hypotheses due to the complex nature of transient phenomena in this area. Techniques for predicting the effect are currently being investigated. With respect to producing the characteristic sound of the rumble events, all three proposed hypotheses would appear to be adequate.

GAS DYNAMICS

Analyses of steady state operation of the LMF upstream test train provide the base operating levels of this system around which transient flowfield phenomena need to be analyzed. The two fundamental areas for which steady state conditions must be reviewed are the operating point of the combustor and the characteristics of the gasdynamics throughout the upstream aerodynamic duct and the diffuser.

Combustor Operation

Using the measured combustor operating data as summarized in Table 2, steady combustor and upstream test train performance was calculated to establish the baseline operating levels around which the transient events occur. These analyses were aimed at determining the ideal combustion process thermodynamics which would occur subject to excursions in the effective area of the flow duct throat. Excursions in the effective throat area is a simple model for the gross flowfield effect of an intermittent entrainment of molten slag from the combustor into the flow stream. That is, when a mass of slag is aerodynamically sheared from the pool that forms in the primary combustion chamber and is drafted through the upstream flow train, this mass can create an physical obstruction to the free plasma flow by blocking the available cross-sectional area within the nozzle and aerodynamic duct. As the slag mass passes through the nozzle throat and subsequently through the aerodynamic supersonic duct, the combustor response will be similar to that caused by a perturbation of the choked throat area. This perturbation will initiate and force a regulation of chamber pressure.

The chamber pressure perturbation caused by slag entrainment will be time dependent. The combustion pressure will rise from its initial state and move toward a new stable point as long as the slag blockage is present anywhere in the upstream flow train. The transient response of the combustion pressure and its net increase over the entire perturbation period are directly proportional to the degree of blockage and the time for which it persists within the duct. Or rather, the time-history of the cross-sectional area obstruction caused by the mass of entrained slag is fundamental in driving the combustion pressure transient. A reasonable approximation of the bounds of the combustor pressure fluctuations (maximum and minimum level) can be achieved through theoretical analyses of the chamber steady state stagnation pressure versus throat area for a choked flow condition.

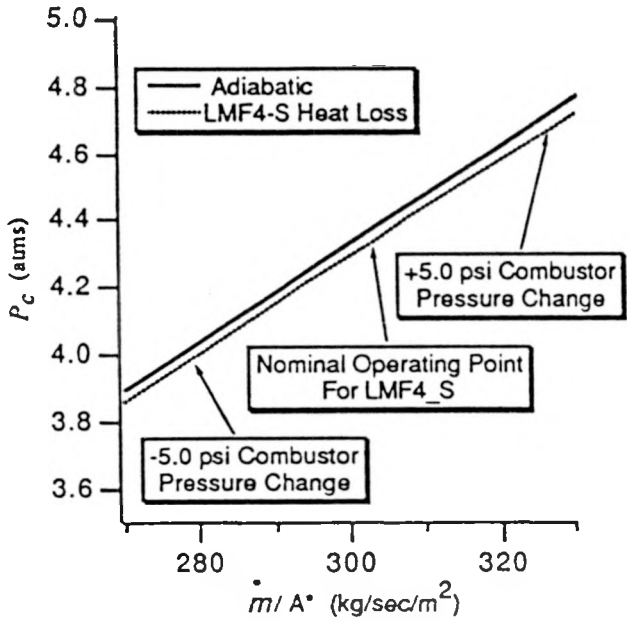

Figure 19.CFFF LMF Combustor Operation - Combustor Pressure Variation with $\dot{m}/A^*$(

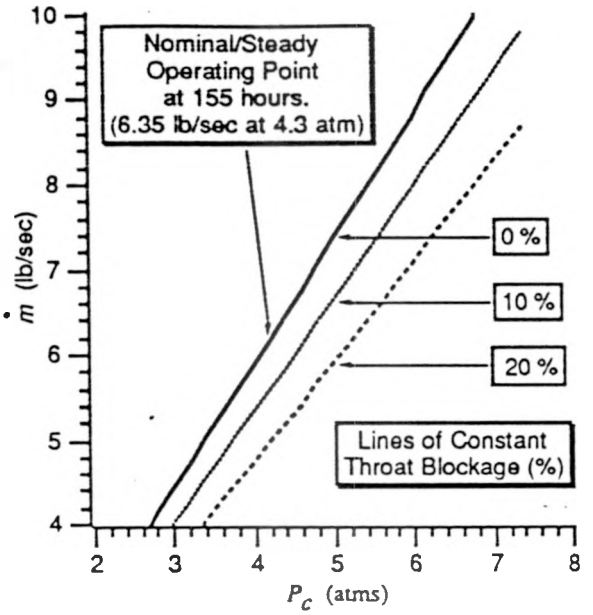

Figure 20. Effect of Nozzle Throat Area Blockage on Combustion Pressure

A graphical representation of this type of steady state combustion pressure behavior for the CFFF LMF system is provided in Figure 19. This figure summarizes the results of thermochemical equilibrium combustion calculations (NASA SP-273) based upon the LMF4-S measured combustor flows (Table 2) along with calculations for the flow expansion process through the nozzle throat. The results depict theoretical combustion chamber pressure as a function of $\dot{m}/A^*$(mass flow rate normalized by the throat area). Two lines are plotted which illustrate the influence of heat loss. The nominal, steady operating point for the LMF system at the conditions of LMF4-S is denoted on Figure 19. Also indicated are points of operation indicating a shift of 5.0 psi pressure about the ideal pressure of the nominal steady state operating point. This magnitude of this pressure fluctuation is of the order of the maximum that was noted in LMF4-S dynamic pressure measurements.

During the transient period that would occur when combustor slag was entrained into the flow and passed through the throat, both the combustion pressure and the net mass flow rate would respond to the presence of a flow obstruction. However, a slag obstruction of the type being considered here is itself dynamic, i.e., the entrained mass moves through the upstream flow train. In this context, provided the slag mass is large enough, the situation which could prevail is that of a dynamic throat. Consequently, the time scale required for the combustor to respond to any slag blockage is an uncertainty which is coupled to the dynamics of the slag itself. However, by reviewing the variation in the abscissa value of the plot of Figure 19 that is consistent with the 5.0 psi pressure change, an approximate indication of the required throat area blockage can be reasoned. That is, for a fixed mass flow rate, a 5.0 psi pressure fluctuation is consistent with a static blockage of the nozzle throat area on the order of 7.0 %.

Figure 20 is an alternate representation showing the effect of throat area blockage on combustor operation. In this figure, pressure is plotted against total mass flow rate for geometrical considerations and conditions consistent with operation of the CFFF during the analysis period of LMF4-S. Three plotted lines are shown for different percentage throat area blockage. Gross throat area changes of 10 and 20% are considered. By moving horizontally across Figure 20 away from the nominal operating point, an indication is obtained of the ultimate combustion pressure that would be achieved for a given throat blockage. In general, for large throat blockages (10 to 20%) large pressure changes are predicted (0.5 to 1.0 atmospheres).

These predicted *steady state* pressure increases (i.e. 1 atm for 20 % blockage) are consistent with the measured dynamic pressure increases (i.e. 1 psi for 22 % blockage existing for 10 ms) simply because the blockage during an event persists for such a brief time.

Steady State Gasdynamics

Intermittent entrainment of molten slag from the combustor will also affect the plasmadynamics in the upstream LMF test train. The test train has two major portions; the aerodynamic duct and the diffuser. Both of these portions are constructed of three duct sections and discontinuities in the flow area distribution occur between these sections. In the case of the diffuser, these discontinuities are intentionally designed to provide abrupt flow field diffusion in the low velocity portion of the diffuser. In the case of the aerodynamic duct these discontinuities represent construction simplicity (fabrication with constant divergence wall angles). As a means of investigating the hypothesis of combustor slag entrainment as the possible source of the acoustic furnace rumbles, two calculations were performed to provide a comparative basis

for the wideband data: nominal supersonic operation and a subsonic condition.

An overview of the normal supersonic steady state plasmadynamics within the upstream LMF test train is given in the plots of Figure 21. These plots present predicted variations in selected thermodynamic and gas dynamic variables along the length of the LMF aerodynamic duct and through the diffuser. Calculations were made using a UTSI design/analysis computer code that has been tailored for application to the LMF test train.[8] The flowfield modeling used is conventional for computing one-dimensional flows. However, special techniques have been incorporated into this particular computer program to account for the presence and effects of a wall slag layer, the effect of dissimilar wall materials on the heat transfer, and to model the shock system. With regard to the latter of these items, for supersonic flow the computer code iterates on the shock position to determine its proper location (i.e., as is required for proper recovery to the back pressure).

The flowfield was computed based upon LMF4-S combustor operation as given in Table 2. This operating point is at a somewhat lower total throughput than that for which the upstream lofting was initially designed. The calculations of this figure depict a supersonic, accelerating flowfield throughout the aerodynamic duct. In this region, the velocity substantially increases as does the Mach number while the static temperature and pressure decrease. As indicated by the abrupt total pressure drop, the flowfield shock structure initiates in the middle portion of the third aerodynamic section and extends the remaining length of this section. Downstream of this shock structure the flow is driven subsonic and eventually exits the upstream as a low velocity, well diffused stream.

The calculations show sensitivity to lofting inflections. Slight discontinuities in the slopes of the various profiles are seen where the various duct sections mate. These discontinuities are real but exaggerated due to the 1-D formulation of the model. Heat transfer data taken for the analysis period of LMF4-S is shown on Figure 21 for comparison to the modeled heat flux. These data represent caloric heat balance calculations computed from cooling water temperature rises across the various cooling rings and sections of the test train. The heat transfer data were the only definitive, standard CFFF facility test data by which the calculated results could be judged. Because of a good comparison betweeen measured and predicted heat flux, these calculations are considered to provide a reasonably good rendition of the actual steady state upstream plasmadynamics.

If slag blockage in the upstream occurs, the worst scenario would be that the entire flowfield within the aerodynamic duct is driven subsonic. Hypothetically, this scenario represents a repositioning of the flowfield throat at the exit of the third aerodynamic duct section. Also for this situation, one limiting case would be that in which the magnitude of the exit blockage is such that the flow within the diverging portion of the nozzle is just subsonic, i.e. the nozzle throat Mach number is essentially unity. Under these ideal conditions, the combustor chamber pressure will remain nearly identical to that experienced with normal supersonic operation.

Subject to the hypothetical case described in the above paragraph, the subsonic calculations shown in Figure 22 were generated. These calculations extend through the aerodynamic duct and are shown in comparison to the supersonic results. The character of the subsonic regime is that of a decelerating flow which is opposite to that for the supersonic flow. Plasma temperature is sustained nearly constant while pressure increases and velocity decreases rapidly.

It is interesting to compare the velocity predictions for both the supersonic and the subsonic calculations to those derived from wideband luminosity data using the phase shift technique discussed earlier. Figure 23 gives a view of the velocity predictions across the aerodynamic duct and notes the axial location where the luminosity measurements were made. The two measurement ports were .4064 meters apart and were centered in the second aerodynamic duct section. The supersonic velocity prediction in this region of the duct is centered around 1284 m/s. This is very near the value of 1300 ± 20 m/s derived from the phase shift of the wideband luminosity signals during a steady period of operation. The subsonic prediction is around 467 m/s. This level is similar to that obtained from the luminosity time shifts of the trailing edge of a rumble event.

SUMMARY AND CONCLUSIONS

An investigation was conducted of the flow disturbances exhibited by the LMF flow train at the CFFF that are characterized by easily audible rumbles and simultaneous dropouts in light emissions and transmissivity across the flow. The purpose of the investigation was to analyze quantitative measurements of parameters that would allow determination of the underlying cause of the flow disturbances. Wide band instrumentation was required due to the short time scale of the phenomena. Instrumentation included three line reversal systems, four helium bleed pressure transducers, two luminosity probes, and an acoustic microphone. Steady state thermodynamic analysis of the flow train at conditions corresponding to measured rumble phenomena were also presented. Suggested causes for the flow disturbances , including coal/seed flow disturbances, combustion instabilities, and slag entrainment into the flow, were evaluated in regards to the data and theoretical analysis.

The experimental data is consistent with a coherent structure that is created upstream of the second section of the aerodynamic duct and then moves downstream eventually reaching the radiant furnace where the effects of the structure have been significantly mediated by diffusion and mixing. The temperature of the structure is possibly below 1900 K and it is definitely opaque over a broad range of visible wavelengths. The latter demands the conclusion of particulate absorption/scattering as opposed to resonant line absorption. Measurements of the structure velocity indicate a length sufficient that the structure can completely fill the upstream aerodynamic duct, indicating a dispersed structure, such as a cloud of particles. Finally, the vitiation heater pressure rise suggests a transient blockage in the upstream components of the flow train.

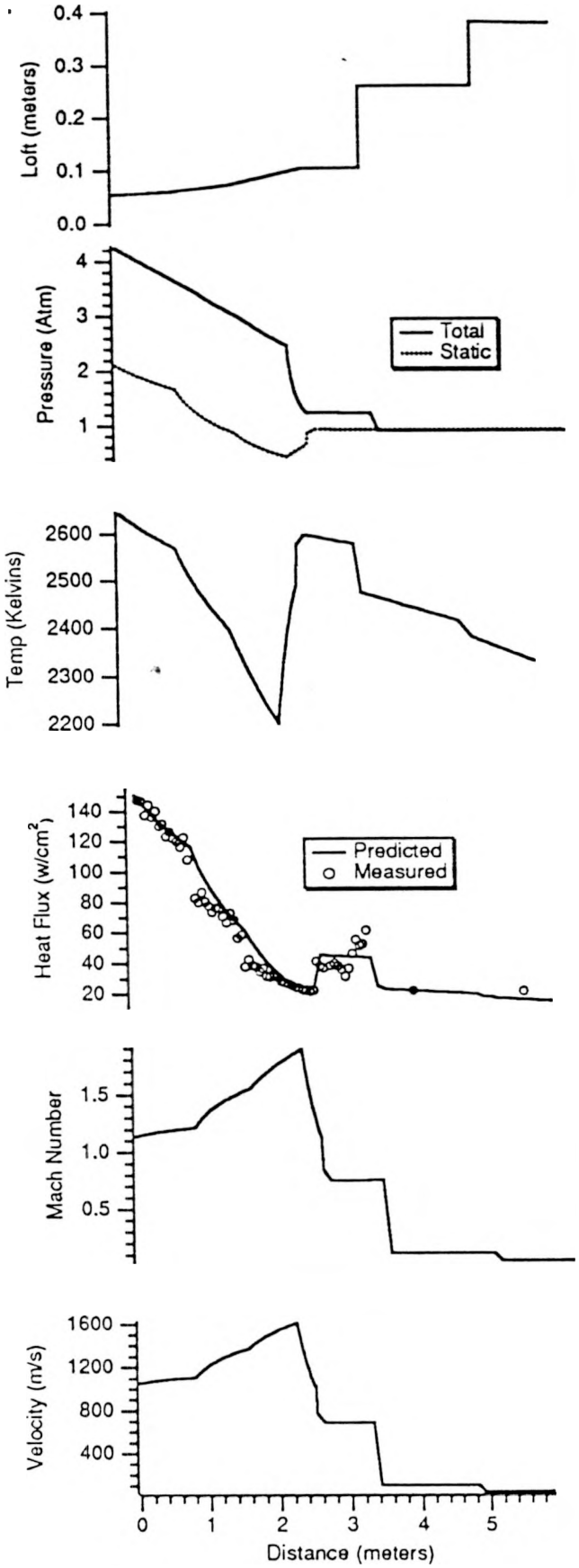

Figure 21. Supersonic Gasdynamics of the LMF Upstream Flow Train

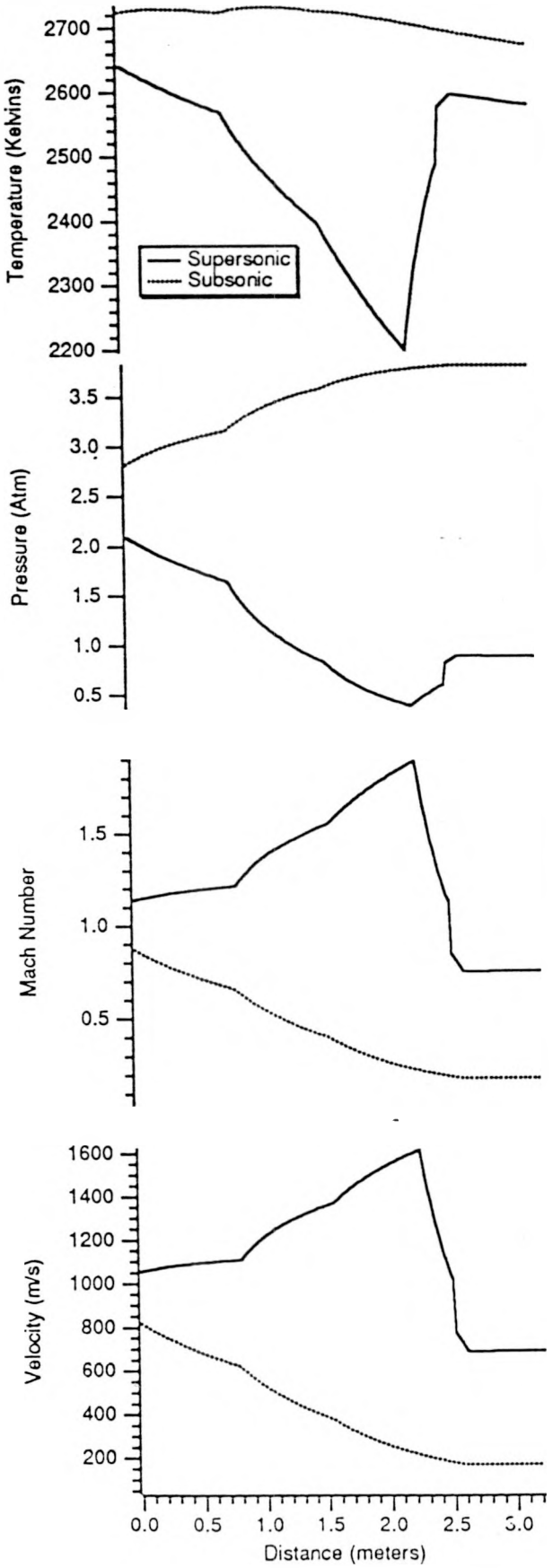

Figure 22. Comparison of Supersonic to Subsonic Operation of the LMF Upstream Flow Train

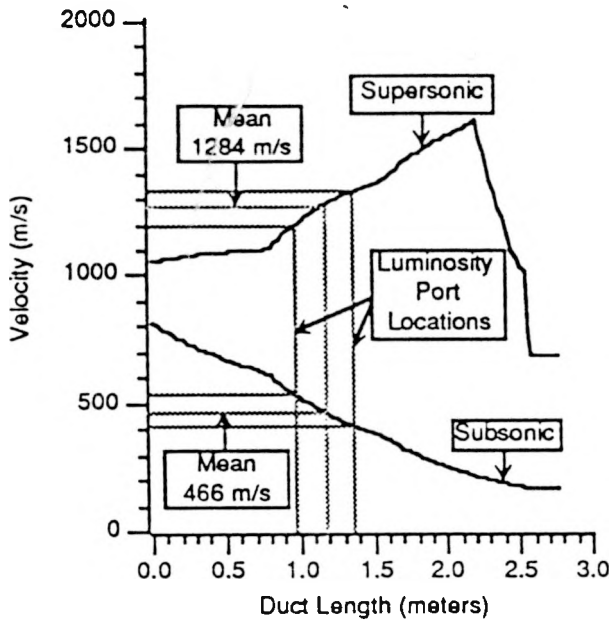

Figure 23. Calculated Duct Velocity.

The coal/seed flow disturbance hypothesis is considered inadequate because it cannot explain the broad band absorption phenomena. Coal combustion loss supplies a cloud of particles to explain the absorption but cannot explain the lack of a pressure drop. Furthermore, a coal combustor flame out is considered unlikely because the vitiation heater exit gas temperature is above the autoignition point for the pulverized coal.

The only objection to the slag entrainment hypothesis is the measured coherent structure length. This can be explained by atomization of the slag into a dispersed mass by the high aerodynamic forces that occur as the slag is entrained from the combustor into the accelerating nozzle and duct flow.

Overall, the steady state calculations presented provide a first order view for interpretation of the acoustic rumble data. These analyses suggest that the hypothesis of slag entrainment as posed for the acoustic rumble source is a strong possibility. The fluctuations in combustion pressure are in keeping with what would occur for intermittent flow blockage if a mass of slag was lifted into and passed through the upstream flow duct. The velocity with which the upstream edge of the dropout in plasma luminance moves through the duct is nearly identical to the flow velocity for supersonic operation while the trailing edge velocity is quite similar to subsonic operation. This observation suggests the presence of an obstruction that creates a "dynamic choke point" which is convected with the flow.

Based on the experimental and theoretical evidence, it is concluded that a dispersed structure of slag particles entrained from the combustor is the most viable hypothesis for explaining the observed flow disturbances.

REFERENCES

1. B.C. Winkleman and T.V. Giel "Non-Simultaneous Sampling Error in Modified Line Reversal Temperature Measurements," Proceedings of the 23rd Symposium on Engineering Aspects of Magnetohydrodynamics, USDOE Pittsburgh Energy Technology Center, Somerset, PA, June 1985, pp 292-301.

2. Data from unpublished test report on the 1981 TP40B test, UTSI.

3. Culick, F.E.C., "Combustion Instabilities in Liquid-Fueled Propulson Systems--An Overview," AGARD 72B PEP Meeting, October 1988.

4. Humphrey, J.W. and Culick, F.E.C., "Acoustic-Energy Interactions in Ramjet Combustion Chambers," AIAA/SAE/ASME/ASEE 23rd Joint Propulsion Meeting, AIAA Paper 87-1872, 1987.

5. Lineberry J. T. and Lee J. J.,"CFFF LMF Radiant Furnace Modelling," 24th Symposium on Engineering Aspects of Magnetohydrodynamics, Butte, MT, June 1986.

6. Wilson W. W., et al., "Laser Doppler Velocimetry Measurements in the CFFF Radiant Furnace," AIAA-89-0226, 27th Aerospace Sciences Meeting, Reno, NV, January 1989.

7. Bendat and Piersol, *Random Data: Analysis and Measurement Procedures*, Wiley-Interscience, New York, 1971.

8. Lineberry, J. T. and Galanga F. L.,"Gas Dynamic and Heat Transfer Evaluations of the CFFF LMF1 Flow Train," 21st Symposium on Engineering Aspects on Magnetohydrodynamics, Argonne National Laboratory, Argonne, IL, July 1983.